The Plant Cell, Vol. 27: 2484–2500, September 2015, www.plantcell.org

Differential Growth in Periclinal and Anticlinal Walls during Lobe Formation in Arabidopsis Cotyledon Pavement Cells

William J. Armour, Deborah A. Barton, Andrew M.K. Law, and Robyn L. Overall[1]

School of Biological Sciences, University of Sydney, NSW 2006, Australia

ORCID ID: 0000-0002-1240-0058 (W.J.A.)

Lobe development in the epidermal pavement cells of *Arabidopsis thaliana* cotyledons and leaves is thought to take place via tip-like growth on the concave side of lobes driven by localized concentrations of actin filaments and associated proteins, with a predicted role for cortical microtubules in establishing the direction of restricted growth at the convex side. We used homologous landmarks fixed to the outer walls of pavement cells and thin-plate spline analysis to demonstrate that lobes form by differential growth of both the anticlinal and periclinal walls. Most lobes formed within the first 24 h of the cotyledons unfurling, during the period of rapid cell expansion. Cortical microtubules adjacent to the periclinal wall were persistently enriched at the convex side of lobes during development where growth was anisotropic and were less concentrated or absent at the concave side where growth was promoted. Alternating microtubule-enriched and microtubule-free zones at the periclinal wall in neighboring cells predicted sites of new lobes. There was no particular arrangement of cortical actin filaments that could predict where lobes would form. However, drug studies demonstrate that both filamentous actin and microtubules are required for lobe formation.

INTRODUCTION

The shape of plant cells is conferred by their surrounding cellulosic cell walls. They can vary from simple, box-like root cells to complex leaf trichomes or the jigsaw puzzle-like leaf epidermal cells of many herbaceous species. The epidermal pavement cells of *Arabidopsis thaliana* leaves and cotyledons are a good model system for understanding how plant cells form complex shapes because their walls develop from simple arcs to contain multiple undulations of varying sizes (Mathur, 2004, 2006; Fu et al., 2005). In a single cell, these undulations, hereafter referred to as lobes, either extend out of the cell (concave lobe) or into it (convex lobe) (Korn, 1976). As lobes are shared between neighboring cells, each lobe has both a concave side and a convex side. During growth, plant cell walls expand either diffusely across a broad area or via tip growth where expansion is restricted to an apex, such as in pollen tubes or root hairs. In pavement cells, it has been proposed that the concave side of lobes form through tip-like growth driven by concentrations of actin filaments at the tip (Fu et al., 2002, 2005; Mathur, 2006; Xu et al., 2010). It is also possible that, to reduce friction, the side walls of lobes grow faster than the tips (Geitmann and Ortega, 2009). The actin filaments at lobe tips are thought to deliver vesicles containing wall precursors and wall loosening enzymes to the developing tips, increasing wall expansion at these sites (Fu et al., 2002, 2005). The importance of actin filaments and actin binding proteins in lobe formation is clear because the pavement cells in a number of Arabidopsis mutants of a signaling cascade upstream of actin filaments have either smaller or no recognizable lobes. Proteins in this cascade include Rho of plants (ROP) and ROP interactive crib motif protein (RIC) (Fu et al., 2002, 2005), ROP guanine nucleotide exchange factor (ROP-GEF) (Qiu et al., 2002; Basu et al., 2008), the actin related 2/3 (ARP2/3) complex (Le et al., 2003; Li et al., 2003; Mathur et al., 2003a, 2003b; Saedler et al., 2004), and the suppressor of cyclic AMP receptor (SCAR) complex (Basu et al., 2004, 2005; Brembu et al., 2004; Zhang et al., 2005, 2008; Le et al., 2006).

Plant cell expansion is perpendicular to the net orientation of cellulose microfibrils in the cell wall (Baskin et al., 1999; Geitmann and Ortega, 2009). Microfibrils are often deposited in the wall in the same direction as microtubules within the cortical cytoplasm because cellulose synthase complexes track along the microtubules (Paredez et al., 2006). Thus, the orientation of cortical microtubule arrays in growing cells can often predict the direction of cell wall expansion (Baskin, 2001). Cortical microtubules are adjacent to thickenings of the anticlinal cell wall on the convex side of lobes in the pavement cells of cowpea (*Vigna unguiculata*) (Panteris et al., 1993a), bird's-nest fern (*Asplenium nidus*), papyrus (*Cyperus papyrus*), *Begonia lucerna*, and maidenhair fern (*Adiantum capillus-veneris*) (Panteris et al., 1994). In Arabidopsis pavement cells, microtubules fan out across the outer periclinal wall from the convex side of lobes (Fu et al., 2002; Qiu et al., 2002; Zhang et al., 2011). Arabidopsis mutants of microtubule-associated proteins such as the CLIP (cytoplasmic linker protein) associated protein (CLASP) or ROP have altered microtubule arrays and their lobes are either broader in shape or fewer in number, indicating that microtubules are required for establishing pavement cell shape (Fu et al., 2005; Ambrose et al., 2007; Ambrose and Wasteneys, 2008). It appears that both filamentous actin and microtubules are involved in lobe development. Indeed, a model where a ROP signaling cascade coordinates alternating areas of tip-like growth at lobes promoted by actin filaments and an inhibition of lobe formation in microtubule enriched regions has been proposed (Fu et al., 2002, 2005; Xu et al., 2010).

[1] Address correspondence to robyn.overall@sydney.edu.au.
The author responsible for distribution of materials integral to the findings presented in this article in accordance with the policy described in the Instructions for Authors (www.plantcell.org) is: Robyn L. Overall (robyn.overall@sydney.edu.au).
www.plantcell.org/cgi/doi/10.1105/tpc.114.126664

The outer periclinal wall is likely to be important in lobe formation. Indeed, Watson (1942) suggested that hardening of the cuticle in localized alternating areas of the outer periclinal surface of ivy (*Hedera helix*) pavement cells inhibited wall growth causing lobes to form in between the areas of hardening. Panteris et al. (1994) showed that during the earliest period of lobe formation in bird's-nest fern cells, when anticlinal walls are straight, there is a gradient of outer periclinal wall thickening with concentrations of cellulose microfibrils adjacent to cortical microtubules that fan out radially across the periclinal wall. They predicted that during cell expansion, wall growth will be restricted at the sites of cellulose microfibril concentrations, causing the convex sides of lobes to form. The fan-like arrangement of cortical microtubules and consequently microfibrils across the outer periclinal wall from the developing convex side of lobes is suggested to reinforce the anisotropic pattern of lobe growth (Fu et al., 2005; Panteris and Galatis, 2005).

Three phases of Arabidopsis pavement cell development have been proposed (Fu et al., 2002, 2005). These authors propose that small cells expand along the long axis of the leaf to form elongated polygons (stage I). Cells enter stage II when lobes start forming, and stage III represents mature cells that are large and highly lobed. Fu et al. (2005) suggest that in stage II, rather than all lobes initiating at once, reiterative lobe formation generates the highly complex shape of stage III cells. These phases of lobe formation have been predicted from observations of cells across a developmental gradient at a single time point (Fu et al., 2002, 2005). Another study that has monitored single Arabidopsis pavement cells over time instead suggests that lobes form in an initial wave that is then followed by a long phase of isotropic expansion indicating lobe formation is discontinuous (Zhang et al., 2011). However cell monitoring began 2 d after germination when many lobes had already initiated. To fully understand the mechanism leading to lobe formation, detailed measurements of periclinal and anticlinal wall growth and corresponding cytoskeletal arrangements during development of individual cells is needed from the earliest possible time.

Through monitoring the same pavement cells of Arabidopsis cotyledons over time immediately after cotyledon unfurling, we demonstrate that most lobes form between 1 and 2 d after germination. Lobes formed via anisotropic expansion of the outer periclinal wall on the convex side of lobes and isotropic expansion on the concave side. Cortical microtubules were enriched on the periclinal wall at the convex side of developing lobes and this arrangement persisted over time. Actin filaments were also concentrated at these sites, but only at later stages of lobe development. On the anticlinal wall, microtubules, but not actin filaments, were concentrated at the tips of developing lobes. Nevertheless, drug studies showed that both actin filaments and microtubules are required for lobe initiation. Our results highlight that differential growth of the outer periclinal wall is important for lobe formation.

RESULTS

Lobe Initiation Is Pronounced during Early Pavement Cell Development

To characterize lobe development in pavement cells, cells from the base of Arabidopsis cotyledons were monitored from 1 to 3 d after germination (for a representative cell, see Figure 1A). Five large, nonadjacent pavement cells, between 350 and 2000 μm^2 in area at day 1, were selected from each of 10 cotyledons and their areas and perimeters were measured at each day (50 cells in total). At day 1 when cotyledons had just unfurled and were first horizontal, the cells were small with short walls and few lobes (Figure 1A). By days 2 and 3, the cells had become more complex in shape with multiple lobes and the mean area and perimeter of the cells had significantly increased while the circularity significantly decreased ($P < 0.001$, repeated measures ANOVA; Figure 1D). The period of fastest cellular growth was between day 1 and 2 when cell areas increased 4 times and perimeters more than doubled, indicating large increases in both periclinal wall areas and anticlinal wall lengths. Growth of the area and perimeter of cells slowed between days 2 and 3 (Figures 1A and 1D). The number of lobes in a cell, including both concave and convex, was counted manually (Figure 1B). The number of concave lobes in a cell was also estimated using an automated approach whereby a cell's shape is reduced to a skeleton outline and the number of skeleton branch ends was counted (Figure 1B) (Le et al., 2006; Zhang et al., 2008, 2011; Staff et al., 2012). Both approaches demonstrated that there was a large increase in the number of lobes between days 1 and 2 ($P < 0.001$, repeated measures ANOVA; Figure 1D). However, the skeleton branch analysis only identifies concave lobes, not convex lobes. Since it did not recognize all concave lobes and identified some wall junctions and straight walls as lobes (Figure 1B), it was not used in further analyses.

To investigate whether there is a relationship between the growth of an anticlinal cell wall segment and the number of lobes that form within it, individual wall segments of the 50 cells were analyzed over the three days. The junctions where three anticlinal walls meet were used to define the boundaries of anticlinal wall segments and three measurements were collected at each time point: the number of lobes per wall segment, the length of anticlinal wall segments, and the Euclidean distance between the wall junctions (Figures 1E and 1F). From day 1 to 2 the average length of anticlinal wall segments increased 2.5 times (slope of line of best fit in Figure 1E), while the average Euclidean distance increased 1.8 times. From day 2 to 3, the comparable measurements were 1.5 (anticlinal wall) and 1.4 (Euclidean distance). Since the length of anticlinal wall segments increased on average more than the Euclidean distance, many of the anticlinal wall segments must have changed shape, especially between days 1 and 2. Change in the length of the anticlinal walls was variable (variation about the line of best fit) at both times, suggesting that when lobes are forming there are many different growth rates (Figure 1E). We then compared the mean number of lobes in an anticlinal wall with its segment length or Euclidean distance and discovered that the length of anticlinal wall or Euclidean distance per lobe was not fixed (Figure 1F). For example, the mean length of anticlinal wall with three lobes at day 1 (40 μm) was approximately the same as the mean length of wall with two lobes on day 2 and one lobe on day 3 (Figure 1F). Correspondingly, the length of anticlinal wall that had three lobes increased from 40 μm on day 1 to 74 μm on day 3, indicating that the lobes became larger and/or further apart over time.

A region of contiguous pavement cells at the base of an Arabidopsis cotyledon was then examined over 3 d to determine

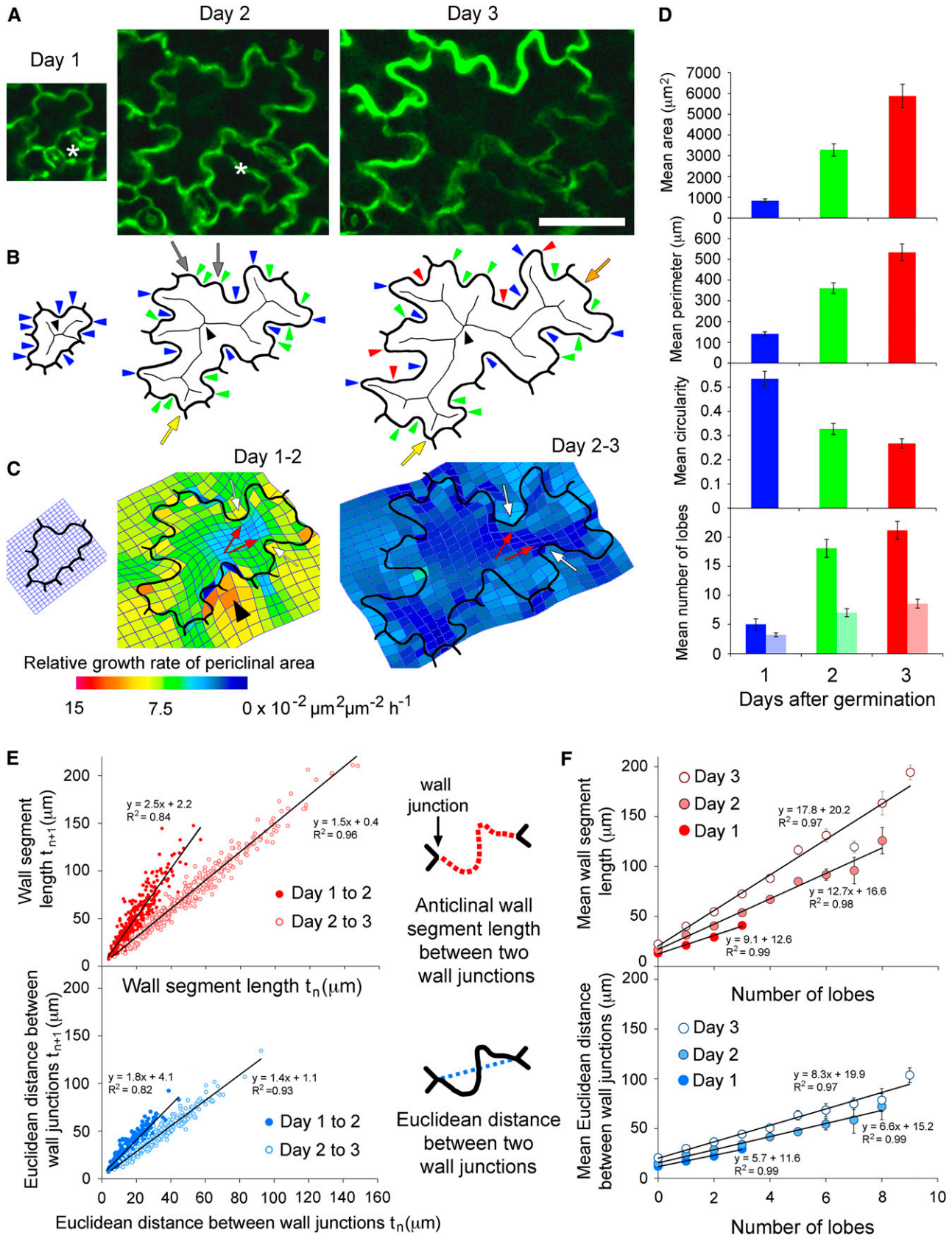

Figure 1. Lobe Development and Growth of Arabidopsis Pavement Cells.

(A) A representative cell at 1, 2, and 3 d after germination. A neighboring cell divided between days 1 and 2 (asterisks). Bar = 50 μm and applies to all three images of the cell between days 1 and 3.

the pattern of coordinated cell growth and development (Figure 2). There was great variety in cell shape and size on each of the days, ranging from large pavement cells to small cells in developing stomatal complexes. The length of each anticlinal wall segment and the periclinal wall area of each cell were determined at each day. Anticlinal and periclinal wall expansion rates varied across the epidermis, with the slowest expansion in guard cells and large pavement cells and the fastest expansion in cells associated with dividing stomatal complexes (Figure 2). Within each pavement cell, anticlinal walls adjoining different neighboring cells grew at different rates, and this variation was independent of the orientation of the walls with respect to the long axis of the cell or the cotyledon (Figure 2). New lobes formed from day 1 to 3 and sometimes developed within existing lobes. Expansion of both the anticlinal and periclinal cell walls was faster between day 1 and 2 than day 2 and 3.

To understand the spatial pattern of growth across the epidermis, we employed thin-plate spline analysis—a technique used to analyze changes in shape and size of objects, for example, in the three-dimensional comparative anatomy of hominid skulls (Rosas and Bastir, 2002; Gunz et al., 2009) or the two-dimensional shape of insect wings (Börstler et al., 2014) or leaves (Polder et al., 2007). The thin-plate spline technique analyzes how the positions of homologous landmarks change between two images and any changes are visualized as warping or deformation of a regular mesh. We observed that the positions of wall junctions linking three anticlinal walls changed from day to day. The positions of these wall junctions were used as homologous landmarks in thin-plate spline analysis to determine the simplest pattern of growth across the epidermis that could explain this movement of junctions. Areas where the wall junctions grew apart (larger polygons in the mesh) coincided with the cells with greatest periclinal wall expansion, particularly the stomatal complexes and their neighboring cells (Figure 2). Similarly, areas where the relative position of the wall junctions did not change (smaller polygons in the mesh) coincided with cells that expanded the least. Growth of periclinal walls in pavement cells showed no net bias in the direction of expansion from day 1 to 2 (square-shaped polygons in the mesh), but when cotyledons became wider from day 2 to 3, periclinal walls expanded preferentially parallel to the width of the cotyledon (rectangular-shaped polygons in the mesh).

Lobes Form via Differential Expansion of the Outer Periclinal and Anticlinal Walls

To gain insights into periclinal and anticlinal wall expansion during lobe formation, fluorescent dots were applied to the surface of cells and their positions were monitored during growth. Dots at or near the join between the anticlinal and outer periclinal walls were used to estimate growth of the underlying anticlinal wall. Anticlinal wall expansion occurred preferentially at sites of lobe formation (Figure 3A). Fortuitous positioning of homologous markers also demonstrated expansion of the periclinal wall during lobe formation (Figure 3B). To visualize growth of the anticlinal and periclinal walls, the positions of homologous landmarks over time were analyzed using thin-plate spline analysis. The relative growth rate of the outer periclinal surface is represented by a color within each polygon of the mesh, while directionality of growth is represented by distortions in the mesh itself. At developing lobes, the relative growth rate of the periclinal wall was greater on the concave side than the convex side, and this differential growth was most pronounced between day 1 and 2 (Figures 3C to 3E). Expansion of the periclinal wall at the concave side of each lobe was relatively isotropic, whereas at the convex side, growth was anisotropic, with the direction of maximal growth being parallel to the tangent to the curve of the anticlinal wall as indicated by the elongated mesh. Growth rates of the anticlinal walls showed a similar pattern to deformations in the mesh, with greater elongation of grid squares corresponding to faster anticlinal wall growth rates (Figure 3E).

As the application of externally applied homologous landmarks to young cotyledons was challenging, an alternative approach for routine thin-plate spline analysis was tested. Each anticlinal wall segment in a representative cell (Figure 1C) was assigned a set number of computed homologous landmarks at day 1, positioned

Figure 1. (continued).

(B) Digital outlines of the cell. Lobes at day 1 (blue arrowheads) and new lobes at day 2 (green arrowheads) and day 3 (red arrowheads) were identified manually. Alternatively, concave lobes were identified at the branch ends of each skeleton (black arrowheads indicate the skeletons). Skeleton branch ends were sometimes present at wall junctions (yellow arrows) or regions of straight wall (orange arrow) and were not always located at small concave lobes (gray arrows).

(C) Thin-plate spline analysis (mesh overlying cell outline) of differential growth in cell walls between days 1 and 2 and days 2 and 3. Periclinal wall growth was predicted to be isotropic on the concave side of lobes (white arrows) and anisotropic on the convex side (red arrows). The region of intense growth (arrowhead) corresponds to the newly divided cell (asterisk in **[A]**).

(D) The mean area, perimeter, and circularity of 50 pavement cells at days 1, 2, and 3. A circularity value of 1 is a perfect circle, and 0 is an infinitely complex shape. The mean number of lobes (concave and convex) within each cell per day was identified manually (dark bars) or the mean number of concave lobes was ascertained by counting skeleton branch ends (light bars). Error bars are SE of the mean.

(E) The length of each anticlinal wall segment between two wall junctions within the 50 pavement cells was compared between successive days. For each wall segment, the Euclidean distance between the two wall junctions was also compared between days.

(F) The number of lobes per mean anticlinal wall segment length between wall junctions or per Euclidean distance between wall junctions on day 1, 2, or 3. Error bars are SE of the mean. The sample sizes on day 3 are: 154 anticlinal wall segments with 0 lobes, 116 with 1 lobe, 46 with 2 lobes, and 10 with 3 lobes; on day 4: 16 anticlinal wall segments with 0 lobes, 72 with 1 lobe, 77 with 2 lobes, 72 with 3 lobes, 48 with 4 lobes, 22 with 5 lobes, 12 with 6 lobes, 4 with 7 lobes, and 3 with 8 lobes; on day 5: 12 anticlinal wall segments with 0 lobes, 45 with 1 lobe, 71 with 2 lobes, 80 with 3 lobes, 57 with 4 lobes, 28 with 5 lobes, 19 with 6 lobes, 4 with 7 lobes, 7 with 8 lobes, and 4 with 9 lobes.

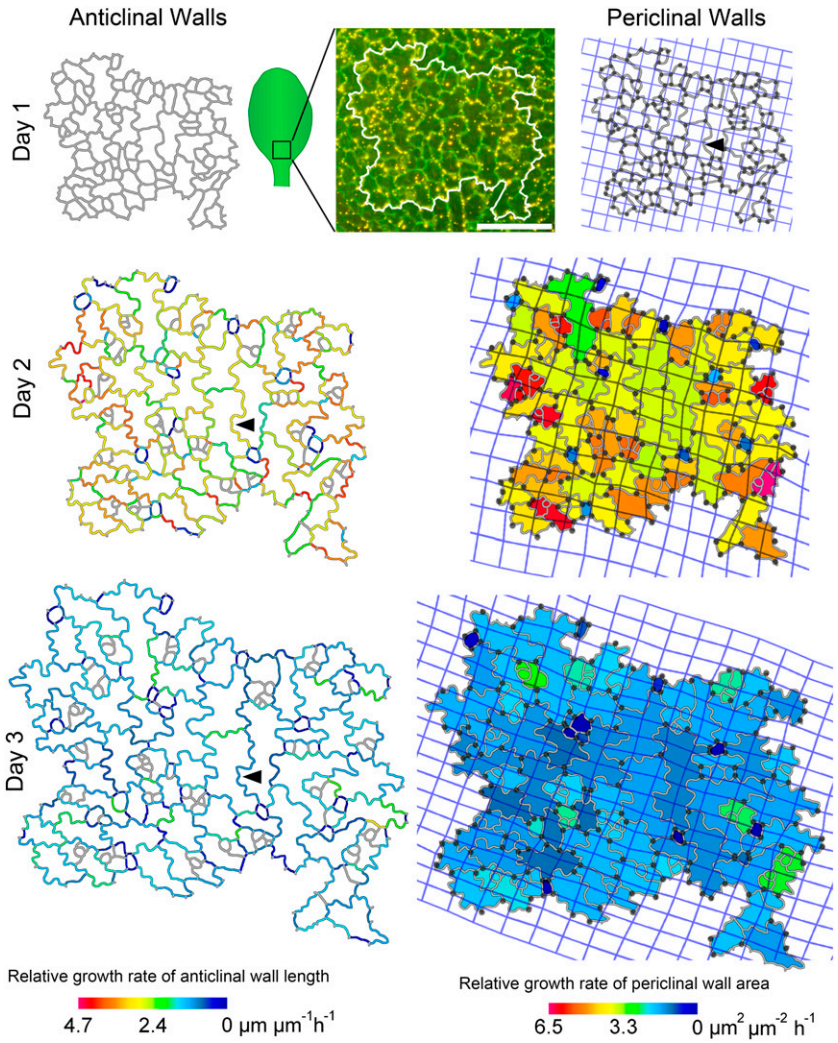

Figure 2. Anticlinal and Periclinal Wall Growth Varies across a Region of Contiguous Pavement Cells.

Fluorescently stained pavement cells at the base of a cotyledon and their digital outlines on days 1, 2, and 3 after germination. The relative anticlinal and periclinal wall growth rates from days 1 to 2 are depicted as a color scale on day 2 images and the growth rates from days 2 to 3 on day 3 images. New anticlinal walls are gray because their growth rates could not be calculated. New lobes sometimes developed within preexisting lobes (black arrowhead). Each thin-plate spline (mesh overlay on the periclinal wall images) models differential movement of the wall junctions (black dots) between days. Bar = 100 μm.

at 0.5-μm intervals (Supplemental Figure 1). To examine development of cell shape, it was assumed that these computed landmarks moved apart equally from day to day in proportion to the increase in length of each anticlinal wall segment. The distance between the landmarks varied within each wall from day to day, with little expansion in stomatal walls and large expansion in the wall of a dividing cell (Supplemental Figure 1). Thin-plate spline analysis of this cell showed that expansion of the periclinal walls at the periphery of the cell was faster than toward the middle (Figure 1C). At lobes, periclinal wall expansion was isotropic on the concave side and anisotropic on the convex side of lobes (Figure 1C), similar to the pattern of lobe growth observed using externally applied homologous landmarks in Figure 3E. This suggests that this approach could be used as an approximation for visualizing changes in outer periclinal wall growth at lobes in cases where it is not possible to use fluorescent homologous markers, for example, when the strong fluorescence of the markers would prevent imaging the weaker fluorescence from GFP-tagged cytoskeletal proteins. To confirm this, we compared the two thin-plate spline approaches and found similar patterns of wall growth between days (Figure 3E; Supplemental Figure 2). Both approaches showed similar patterns of wall growth, with differential growth on either side of the lobes on day 1 to 2. From day 2 to 3, both approaches showed lower relative growth rates across the periclinal wall and lobes displayed little change in shape. Since it was possible to predict regions of differential growth on either side of a lobe using computed landmarks for thin-plate spline analysis, this approach was employed for the following cytoskeletal studies.

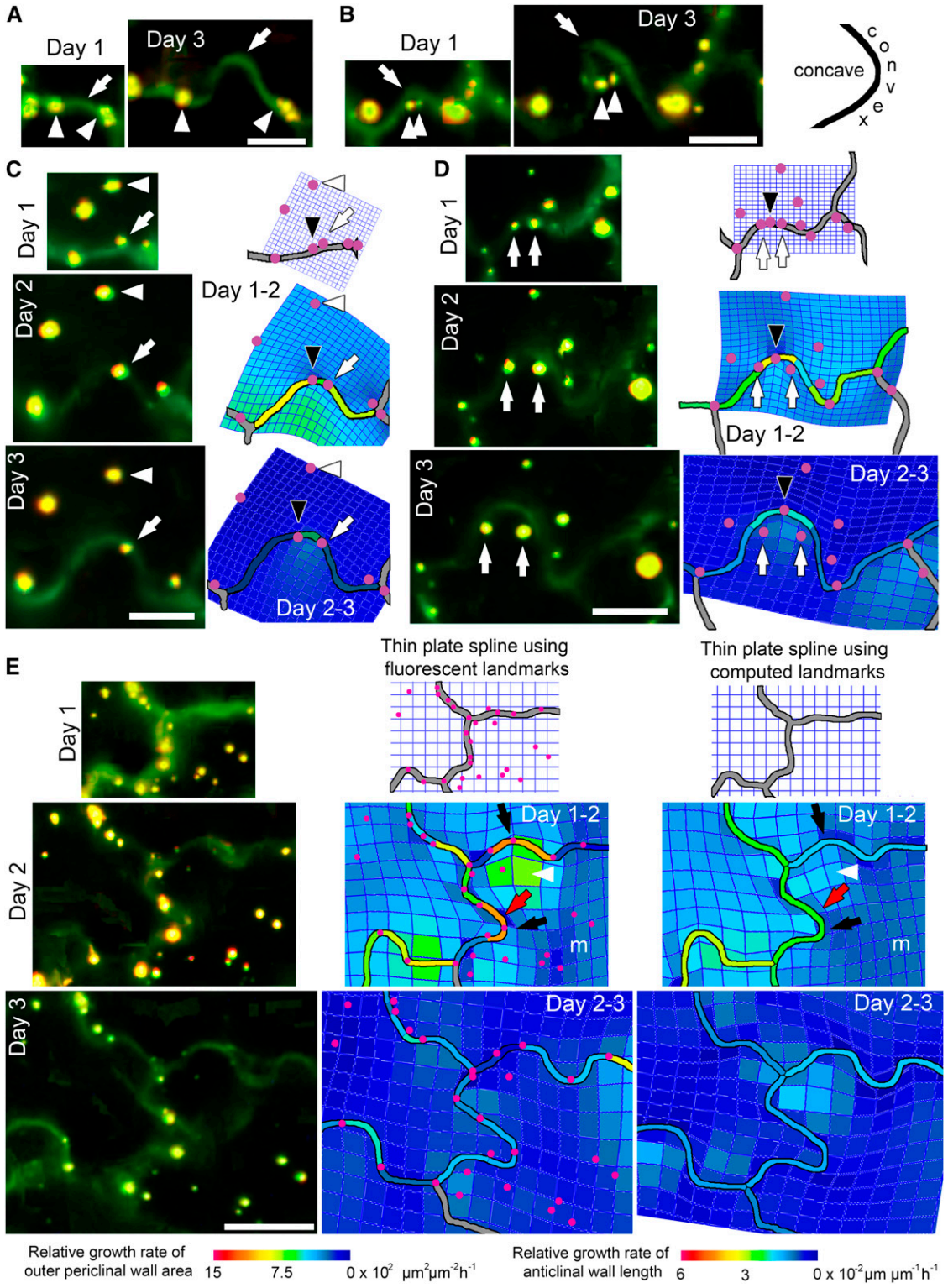

Figure 3. Differential Growth of the Outer Periclinal and Anticlinal Walls at Lobes during Development.

Anticlinal walls (green) and the position of externally applied fluorescent markers on the outer periclinal wall (yellow) during lobe formation from 1 to 3 d after germination from selected walls in Figure 2. Thin-plate spline analysis (mesh) depicts growth of the outer periclinal wall by comparing the positions of

Microtubules, Not Actin Filaments, Persistently Associate with Developing Lobes

To investigate whether microtubules and/or actin filaments are associated with lobes during their development, Arabidopsis plants expressing GFP tagged to β-tubulin 6 (GFP-TUB6) (Nakamura et al., 2004) or GFP tagged to the second actin binding domain of fimbrin (GFP-fABD2) (Sheahan et al., 2004) were used to visualize microtubules or actin filaments respectively in pavement cells. Cells were imaged over 3 d, then their shapes were traced digitally and thin-plate spline analysis was used to predict regions of differential wall growth. The arrangement of cytoskeletal filaments in the cortical cytoplasm of pavement cells at each time point was compared with the predicted periclinal wall expansion. It should be noted that correlations of the cytoskeleton with growth are limited by the fact that the arrangements of the cytoskeleton could only be imaged at discrete time points, while growth is averaged over the interval between imaging.

Across all days, microtubules formed arrays in the cortical cytoplasm next to the outer periclinal wall and adjacent to anticlinal walls (Figure 4A). At day 1, when pavement cells had few lobes, microtubules next to the outer periclinal surface were not coaligned in a single direction (Figure 4A). At later stages of development, microtubules aligned parallel to the short axis of the cell and concentrated where periclinal wall expansion was restricted. Periclinal wall expansion was greatest at sites of lobe growth at the cell periphery. Figures 4B and 4C depict the development of lobes from essentially straight walls on day 1. Microtubules adjacent to the outer periclinal wall were persistently enriched at the convex side of the lobes and were oriented perpendicular to the lobe margin at its convex side. These microtubules at the outer periclinal wall often extended down the anticlinal wall at the convex surface of lobe tips. By contrast, few microtubules were present at the complementary concave side of lobes during development (Figures 4B and 4C). By combining the distribution of microtubules at the periclinal surface of the lobes with the thin-plate spline analysis for these regions, it is evident that expansion of the periclinal wall was greater in the concave side of the lobes where few microtubules were present and was restricted around the convex side of lobes where microtubules were enriched (Figures 4B and 4C).

To ascertain whether microtubules were consistently enriched at lobe tips, microtubule fluorescence intensities at periclinal and anticlinal walls were measured (Figure 4D) in five cells, each from a different plant. At the periclinal wall, there was significantly more microtubule fluorescence on the convex side of lobe tips than the concave side ($P < 0.05$, two-sample *t* test; Figure 4E). This pattern was established at day 1 and persisted throughout development. Microtubules at the anticlinal wall were associated with lobe tips at day 1 and were significantly enriched at the tips except at day 2 ($P < 0.05$, two-sample *t* test; Figure 4E). It was noticed that a band of microtubules at the periclinal wall on day 1 in Figure 4C was oriented perpendicularly to a site on a curved anticlinal wall where after 7 h a lobe had formed. This suggests microtubule bands may determine where a new lobe forms and led us to investigate whether microtubules in other cells predict sites of lobe formation. In Figures 5A to 5C, straight regions of anticlinal wall on day 1 where microtubule bands extended across the anticlinal and periclinal walls subsequently developed into lobes. In addition, at later times where new bands of microtubules appeared at straight regions of anticlinal wall, new lobes also formed (Figures 5B and 5C). Few microtubules were present at the periclinal cortical cytoplasm in neighboring cells opposite these bands. Lobes did not form where bands of periclinal microtubules met on either side of anticlinal walls in neighboring cells (Figure 5D).

Filamentous actin was dispersed throughout the cortical cytoplasm next to the outer periclinal wall during pavement cell development (Figure 6A). Actin filaments showed no clear pattern of enrichment and were found on both the concave and convex sides of developing lobes (Figure 6B). Actin filament fluorescence intensities at lobes were then quantified (Figured 6C and 6D). At the first two time periods, there was no significant enrichment of actin filament fluorescence at either the convex or concave side of lobe tips on the periclinal wall ($P > 0.05$, two-sample *t* test; Figure 6D), but by days 2 and 3, actin filaments were significantly enriched on the convex side of lobes ($P < 0.05$, two-sample *t* test). Close examination revealed thick actin filament bundles extended from the convex side of some lobes (Figure 6B; Supplemental Figure 3), with orientations similar to microtubule bands at comparable sites (Figures 5A to 5C). Apart from day 2, there was no significant

Figure 3. (continued).

homologous landmarks (fluorescent markers, wall junctions, and lobe tips; represented as magenta dots) over time. The relative growth rate of anticlinal wall segments between homologous landmarks is shown by the color overlay on the anticlinal walls.

(A) Lobe formation (arrows) between two fluorescent markers (arrowheads) demonstrating anticlinal wall growth. Bar = 10 μm.

(B) During development of this lobe, two fluorescent markers (arrowheads) originally positioned near the lobe tip move a similar distance away from the tip (arrows), demonstrating periclinal wall growth. The diagram on the right illustrates the position of the convex and concave sides of a lobe. Bar = 10 μm.

(C) A fluorescent marker (arrow) on the anticlinal wall near a lobe tip (black arrowhead) remains at a relatively constant distance from a second marker (white arrowhead) on the convex side of the lobe during lobe formation. Thin-plate spline analysis shows restriction of periclinal wall growth on the convex side of the lobe (blue) and promotion of growth on the concave side (green). Bar = 10 μm.

(D) Development of two lobes depicted by thin-plate spline analysis. Growth of the periclinal wall is promoted at the concave side of the lobes as demonstrated by the displacement of two fluorescent markers (arrows) from the anticlinal wall at a lobe tip (black arrowhead). Bar = 10 μm.

(E) Lobe development in multiple cell walls investigated using two thin-plate spline approaches: (1) using externally applied landmarks and (2) using computed landmarks positioned along the anticlinal wall (landmarks not shown; for an example, see Supplemental Figure 1). Between days 1 and 2, there is differential growth of the periclinal walls with anisotropic growth at the convex side of developing lobes (black arrows) as shown by elongated mesh, which was sometimes skewed to one side of a lobe (red arrows). Growth of the periclinal wall is greatest at the concave side of lobes (arrowheads) and slower in the middle (m) of cells. The distances between externally applied homologous landmarks showed that anticlinal wall segment growth rates varied along a wall with greatest rates at lobe tips. In the thin-plate spline analysis using computed landmarks, it was assumed that growth of each anticlinal wall segment was at a constant rate and these rates varied between walls. From day 2 to 3, growth of anticlinal and periclinal walls was slower. Bar = 50 μm.

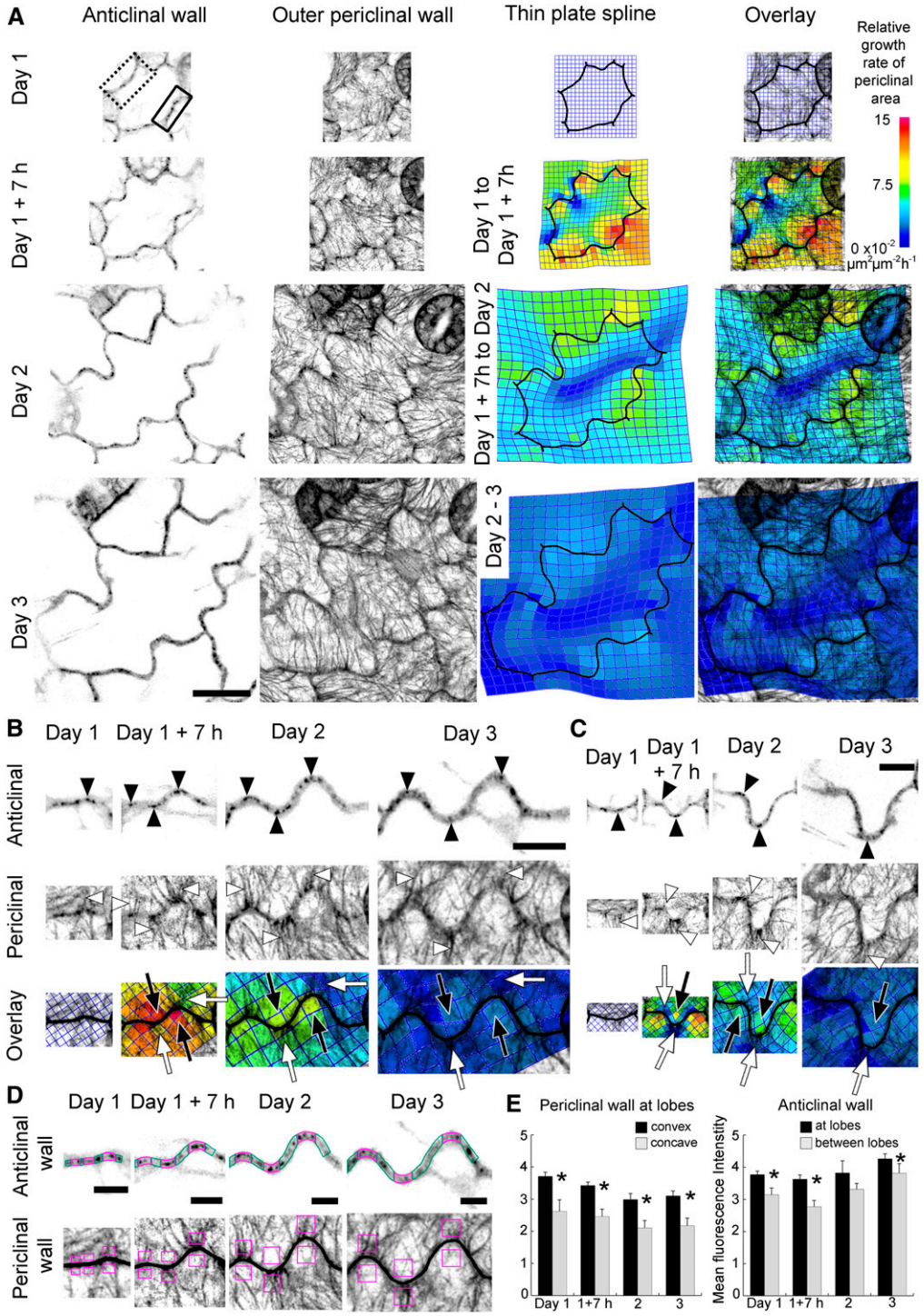

Figure 4. During Pavement Cell Development at the Periclinal Wall, Microtubules Associate with the Convex Side of Lobes and Microtubule Free Zones Persist at the Concave Side of Lobes.

The arrangement of microtubules and growth of cell walls during lobe development in pavement cells expressing GFP-TUB6 from 1 to 3 d after germination. Fluorescence images are optical sections of the anticlinal wall at the middle of the cell and projections of serial sections of the cortical cytoplasm next to the outer periclinal wall. Thin-plate spline analysis predicts relative growth rates in the outer periclinal wall between consecutive time periods.

(A) Microtubule arrangements during the development of a representative pavement cell from 1 to 3 d after germination. In the overlays, concentrations of microtubules correlate with regions of relatively slower periclinal wall growth. Bar = 20 µm.

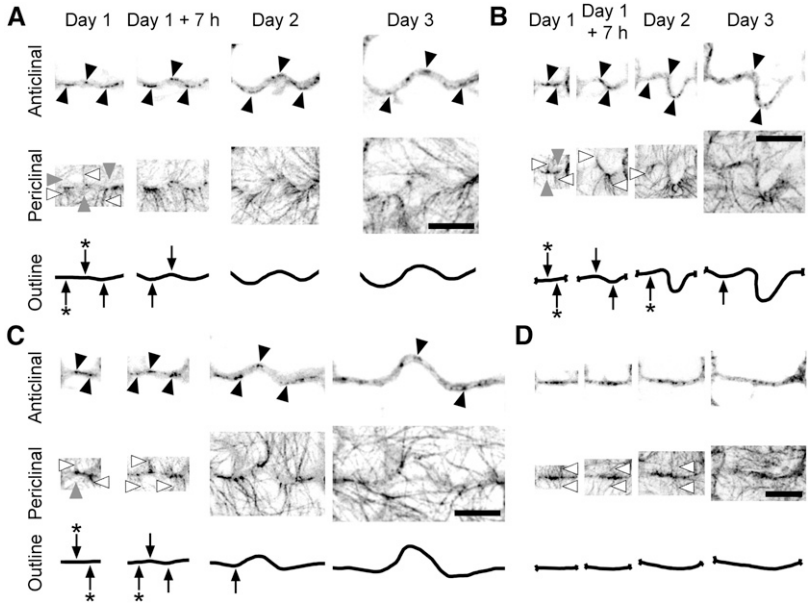

Figure 5. Microtubule Banding Predicts the Growth of New Lobes.

Microtubule arrays at four walls during lobe development of pavement cells expressing GFP-TUB6 from 1 to 3 d after germination. Fluorescence images are optical sections of the anticlinal wall at the middle of the cell and projections of serial sections of the cortical cytoplasm next to the outer periclinal wall. Microtubules were present as bands at the anticlinal wall surface (black arrowheads) and were continuous with microtubules at the outer periclinal cortex region (white arrowheads). Microtubules were less concentrated or absent at the outer periclinal concave region (gray arrowheads). Straight areas of wall enriched with microtubules (black arrows marked with an asterisk) developed into lobes over time (black arrows). Bars = 10 μm.

(A) A wall with three bands of microtubules at day 1. Two bands on the left are part of a straight section of wall that starts to curve into two lobes by day 1 +7 h. The band of microtubules on the far right is associated with a lobe that is already growing.

(B) This straight wall has two bands of microtubules that mark the sites where lobes start developing at day 1 +7 h. At day 2, another band of microtubules appears on the left and a new lobe is forming here on day 3.

(C) A straight wall has two initial bands of microtubules. By day 1 +7 h, these two locations are becoming lobes while a new third band appears for the first time. A lobe forms at this third location by day 2.

(D) A wall with bands of microtubules that met on either side of the anticlinal wall on day 1, 1 +7 h, and 2 changed little in shape from day 1 to 3.

enrichment of actin filaments at lobe tip regions of the anticlinal wall ($P > 0.05$, two-sample *t* test; Figure 6D).

Depolymerization of Actin Filaments and Microtubules Affects Pavement Cell Shape Development

To explore the role of the cytoskeleton in the early stages of lobe formation further, actin filaments or microtubules were depolymerized in wild-type plants at day 1 and growth of the cells was assessed on days 2 and 3. Wild-type plants were used instead of plants expressing cytoskeletal GFP fusion proteins because any potential differences in growth of these lines could confound growth measurements. However, plants expressing the GFP fusion proteins were used initially to determine the length of treatment time required to depolymerize microtubules or actin filaments on day 1 and monitor their recovery. Microtubules were depolymerized with oryzalin (Supplemental Figure 4) and actin filaments with cytochalasin D (Supplemental Figure 5) but both

Figure 4. (continued).

(B) and **(C)** Formation of lobes from two anticlinal walls (the solid and dashed line boxes in **[A]**) at higher zoom. At the anticlinal wall, cortical microtubules associate with the convex side of lobe tips (black arrowheads) during development and extend to the periclinal wall, where these microtubules fan out from the convex side of lobes (white arrowheads). Thin-plate spline analysis predicts that periclinal wall growth is slower at the convex side of lobes, which have bands of microtubules during development (white arrows), and is faster at the concave side of lobes, where microtubules are less concentrated or absent (black arrows). Bars = 10 μm.

(D) Microtubule fluorescence intensities were measured for the anticlinal wall at lobe tips (areas at lobes outlined in magenta) and other regions of the wall (areas between lobes outlined in green). Fluorescence intensities at the periclinal walls on the concave side of lobes were compared with those on the convex side (areas within magenta boxes). Bars = 5 μm.

(E) The average microtubule fluorescence intensities at lobes within cells, including the cell in **(A)**, measured as in **(D)**, at each time point are represented with standard errors. Statistical significant differences within a time point are denoted by an asterisk ($P < 0.05$, two-sample *t* test). Seven lobes were chosen per cell and one cell per plant. $n = 4$ plants at day 1 and 5 plants at day 1 +7 h, day 2, and day 3.

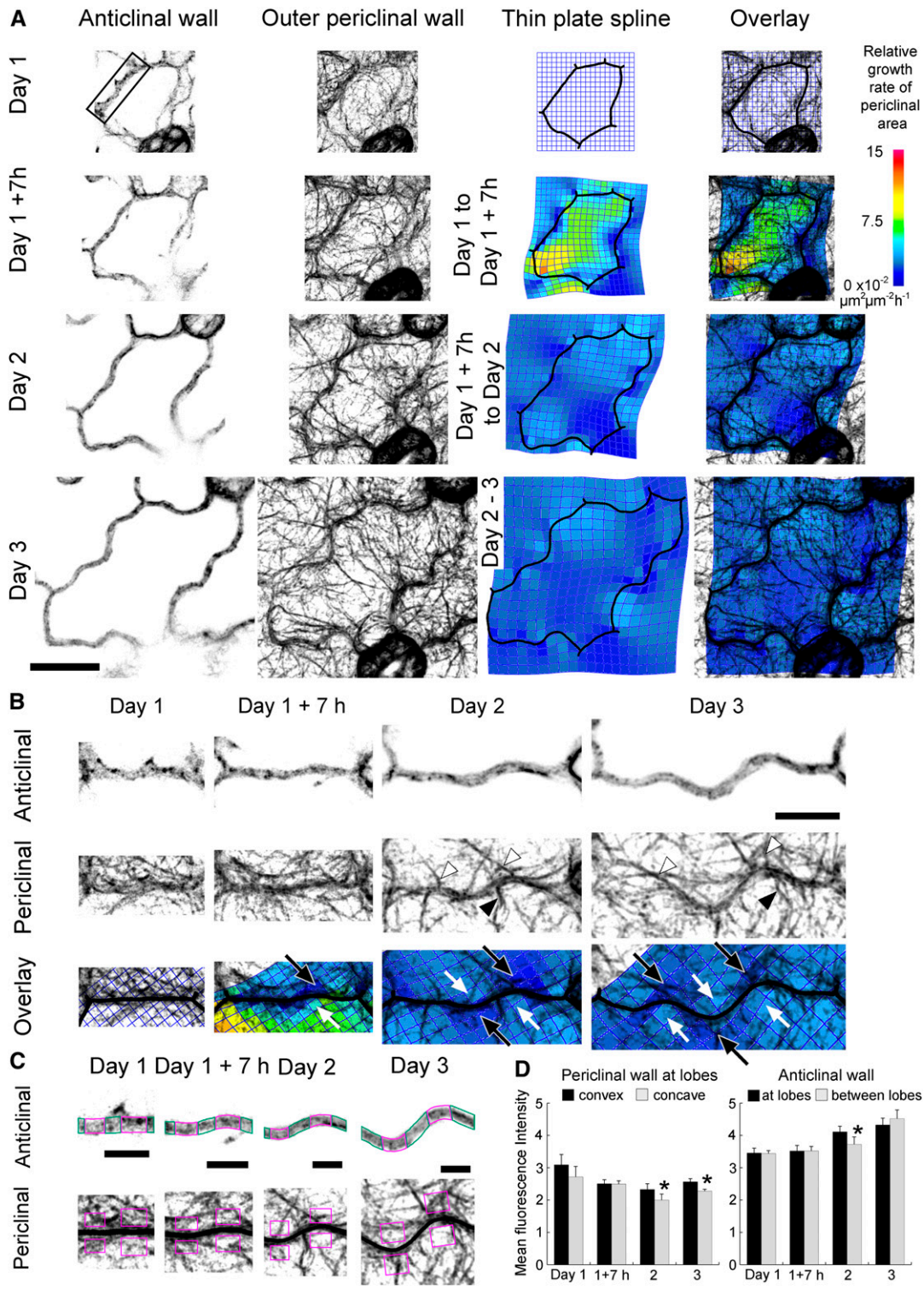

Figure 6. Actin Filaments Do Not Strongly Associate with Either Side of Lobes during Development of Pavement Cells.

The arrangement of actin filaments and cell wall growth in pavement cells of GFP-fABD2 seedlings from 1 to 3 d after germination. Fluorescence images are optical sections of the anticlinal wall at the middle of the cell and projections of serial sections of the cortical cytoplasm next to the outer periclinal wall. Thin-plate spline analysis predicts relative growth rates of the outer periclinal wall between consecutive time periods.

recovered 48 to 72 h after rinsing. Since both of these inhibitors were dissolved in DMSO, DMSO controls (Supplemental Figures 4 and 5) were included and there was no effect on the microtubules or actin filaments.

Control pavement cells and those treated with oryzalin, cytochalasin D, or DMSO increased in size across all days (Figure 7A), which is reflected in their increases in area and perimeter between each day (Figure 7B). The circularity of control cells decreased over the three days, and this corresponded with a significant increase in the number of their lobes from day to day (Figure 7B). Cells of the two DMSO controls had similar changes in area, perimeter, circularity, and number of lobes compared with the controls and these were not significantly different apart from one DMSO control value on day 1. Increases in the amount of lobes and change in lobes per perimeter of the 0.25% and 1% DMSO control were similar to their controls between days.

Cells treated with cytochalasin D and oryzalin were significantly smaller in area and perimeter on days 2 and 3, were more circular in shape, and contained fewer lobes than control cells (Figures 7A and 7B). Oryzalin-treated cells typically did not change shape and their circularity value did not change over the three days. To determine whether lobe formation was being specifically disrupted by oryzalin or cytochalasin D treatment or was a product of overall inhibition of cell growth, the change in the number of lobes per cell perimeter was compared between days. From day 1 to 2, the number of lobes per perimeter increased by approximately the same proportion for the control and DMSO control cells. In comparison, fewer lobes per perimeter were generated in cells treated with cytochalasin D and particularly with oryzalin (Figure 7B), suggesting that lobe development was specifically disrupted. From day 2 to 3, the change in the number of lobes per perimeter was reduced and there was no significant difference between the treatments. Thin-plate spline analysis showed that the outer periclinal walls of representative control and DMSO control cells had similar patterns of differential expansion across the lobes and a restriction of growth in the middle of the cell (Figure 7A). By contrast, change in cell shape of the oryzalin- and cytochalasin D-treated cells was inhibited with deformations in the mesh less pronounced across the lobes and in oryzalin treated cells growth in the middle of the cell was less restricted (Figure 7A). Collectively, the data suggest that disruption of actin filaments with cytochalasin D or microtubules with oryzalin at day 1 hindered the formation and development of lobes by day 3.

DISCUSSION

To understand the mechanism and timing of lobe formation in Arabidopsis pavement cells, we monitored individual cells over three days, from the earliest stages of cotyledon emergence. The morphology of the cells at each day is comparable to the stages of pavement cell shape development defined by Fu et al. (2002, 2005) for Arabidopsis leaves. Cells at 1 d after germination are comparable to late stage I/early stage II cells, which are just starting to form lobes, while cells at day 2 have grown rapidly and produced a large number of lobes (stage II). Cells at day 3 are larger than at day 2 but growth was slower between these days and fewer lobes were formed, potentially indicating a transition to mature stage III cells. Surprisingly, we discovered that pavement cells generated most new lobes within the first 24 h after the cotyledons unfurled (1 to 2 d after germination) during the period of fastest cell growth. During a second 24 h (2 to 3 d after germination), growth slowed and lobe formation reduced. A previous time-course study of lobe development in Arabidopsis cotyledons monitored cells from 2 to 18 d after germination (Zhang et al., 2011). While new lobes formed from day 2 to 3, they rarely initiated after day 3 during a long phase of isotropic cell expansion (Zhang et al., 2011). Our data confirm that the initiation and growth of new lobes does not continue indefinitely.

Epidermal cells in Arabidopsis leaves display large variations between contiguous cells in the relative growth rates of both cell area and anticlinal wall growth when lobes are forming (Asl et al., 2011; Elsner et al., 2012; Kalve et al., 2014). However, it has been suggested that cells in the cotyledon may not have this large growth rate variation in both the cell area and anticlinal wall lengths (Zhang et al., 2011; Elsner et al., 2012). The cells studied here confirm that Arabidopsis cotyledon pavement cells grow similarly to the leaves (Asl et al., 2011; Elsner et al., 2012) as there are patches of different relative growth rates for cell area and anticlinal walls between contiguous cells. There was also a relationship between the length of an anticlinal wall segment and the number of lobes that formed within it at each day, suggesting faster growth rates of the walls are related to increasing numbers of lobes that form within them. Despite the differences in the expansion of individual cell areas, as the anticlinal wall is a shared structure right from its initial formation, this supports the postulate that growth is directed at the level of these shared walls rather than within a cell (Jarvis et al., 2003; Elsner et al., 2012).

Figure 6. (continued).

(A) Filamentous actin in a representative pavement cell from 1 to 3 d after germination. On all days, actin filaments were distributed throughout the cortical cytoplasm. Bar = 20 μm.

(B) Development of three lobes from a relatively straight wall (the boxed region in **[A]** at higher zoom). Relative growth rates in the outer periclinal wall were promoted on the concave side of forming lobes (white arrows) and were restricted on the convex side of lobes (black arrows). Bundles of actin filaments were at both the concave (black arrowheads) and convex (white arrowheads) side of lobes. Bar = 10 μm.

(C) Fluorescence intensity of actin filaments at the anticlinal wall was measured at lobe tips (areas at lobes outlined in magenta) and other regions of the wall (areas between lobes outlined in green). Fluorescence intensity of the filaments was measured in the cortical cytoplasm adjacent to the periclinal wall (areas within the magenta boxes) on the concave and convex sides of lobes. Bar = 5 μm.

(D) Average actin filament fluorescence intensities at lobes within cells, including the cell in **(A)**, measured as in **(C)**, are represented for each time point with standard errors. Statistically significant differences within a time point are denoted by an asterisk ($P < 0.05$, two-sample *t* test). Seven lobes were chosen per cell and one cell per plant. $n = 5$ plants at each time period.

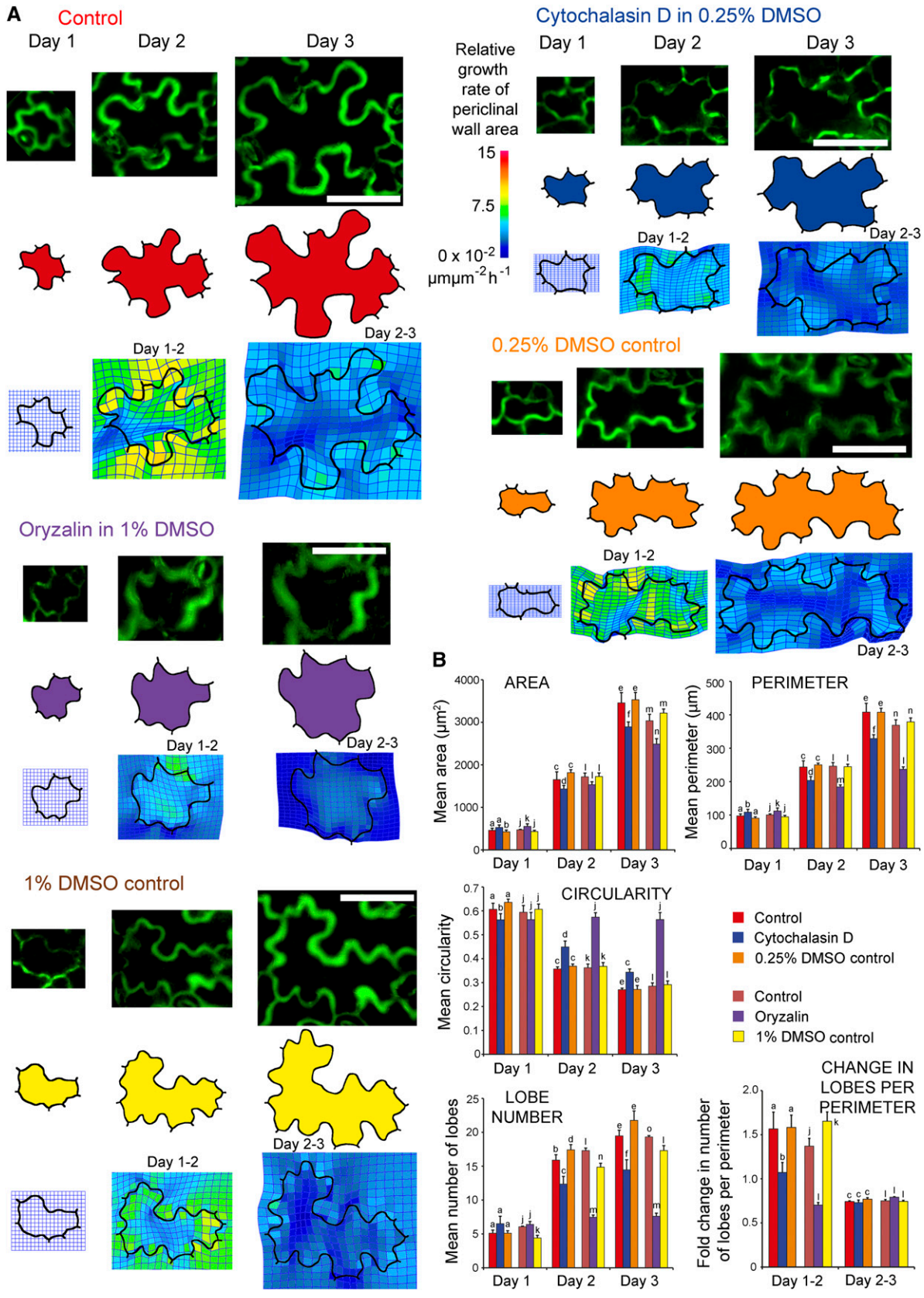

Figure 7. Effect of Cytoskeletal Inhibitors on Pavement Cell Development.

(A) Comparison of pavement cell development from 1 to 3 d after germination between control cells and cells treated with the cytoskeletal inhibitors, cytochalasin D or oryzalin, or their corresponding DMSO controls. For each cell, the top row of images shows anticlinal wall and lobe development, the

The thin-plate spline technique was an effective method to analyze changes in cell shape associated with lobe formation. The two approaches, using applied or computed homologous landmarks, provided similar pictures of differential growth of the walls. Previously, computed homologous landmarks were used to analyze the changes in leaf shape over time, and 46 landmarks were sufficient to define the shape of a leaf margin (Polder et al., 2007). Here, the shape of a pavement cell was defined by more than 200 computed landmarks, and, assuming constant growth along an anticlinal wall, the density of these landmarks allowed us to predict how relative growth rates in periclinal walls varied during lobe formation. Application of external fluorescent landmarks to the periclinal cell wall provided a more realistic indication of how the periclinal and anticlinal walls grew, but it was a random process with little control over the site or the density at which the landmarks attached. We targeted walls with the greatest number of uniformly dispersed fluorescent landmarks near growing lobe tips for thin-plate spline analysis. The total number of applied and morphological landmarks ranged from 6 to 37 per analysis and is similar to the number of landmarks used for other two-dimensional shapes, for example, 13 morphological landmarks for insect wings (Börstler et al., 2014). Unfortunately, the small number of fluorescent landmarks did not allow high-resolution calculation of the subcellular wall growth during lobe formation but it does provide an approximation of the differential growth rates of pavement cell walls during their development. Further resolution of the wall growth at lobes will be important to understand how walls modulate their growth during this cell shape change (Szymanski, 2014).

Thin-plate spline analysis predicted that lobes form by the combination of differential growth in both the periclinal and anticlinal walls. Expansion of the periclinal wall was faster and relatively isotropic on the concave side of lobes. The expansion of the periclinal wall on the convex side of lobes was anisotropic with growth restricted perpendicular to the anticlinal wall where fan-like arrangements of microtubules in the cortical cytoplasm persisted. This finding was predicted by Panteris and Galatis (2005), who suggested that if the often observed fan-like arrangement of microtubules (Panteris et al., 1993a, 1993b, 1994; Wasteneys et al., 1997; Fu et al., 2002; Qiu et al., 2002) is mirrored by the pattern of cellulose microfibril deposition in the outer periclinal wall, the microfibrils would restrict growth parallel to their orientation. Providing this arrangement of microtubules, and consequently microfibrils, persisted, this would cause the outer periclinal wall to curve to form the convex side of a lobe. Indeed, microtubules were found to persist in a fan-like arrangement during lobe development from when a wall was straight until the same region of wall curved into a lobe. A recent study showed that physical stresses in the outer periclinal wall are in a fan-like arrangement at the convex side of lobes, similar to the pattern of cortical microtubules (Sampathkumar et al., 2014). Microtubules are known to align to the direction of maximal stress and their orientation alters to match new directions of stress, for example, during development (Hamant et al., 2008; Burian et al., 2013) or after the application of pressure or wounding (Hush et al., 1990; Hush and Overall, 1991; Sampathkumar et al., 2014). Since microtubules were persistent at the same lobes during their development, it suggests the direction of stresses was maintained in the periclinal wall at the convex side of lobes from day 1 to 3. However, as lobes continue to mature between days 3 and 5, this fan-like arrangement of microtubules can be lost (Zhang et al., 2011), suggesting microtubules may not always follow the stress patterns at lobes in later stages of development (Sampathkumar et al., 2014).

Studies of microtubule arrangements in cowpea pavement cells (Panteris et al., 1993a, 1993b, 1994; Panteris and Galatis, 2005) suggest that microtubule foci extending across the periclinal and anticlinal faces of a cell may predict sites of future lobe formation and must persist at these sites throughout development for the lobes to form. The microtubule-associated protein CLASP, which enables microtubules to span between the outer periclinal and anticlinal faces of a cell, is distributed at discrete foci along straight anticlinal walls in young pavement cells and could be instrumental in determining the sites of microtubule enrichments at forming lobes (Ambrose et al., 2011). Here, we showed that foci of cortical microtubules on straight walls at day 1 predict sites where new lobes form and these microtubules remain enriched at the periclinal wall on the convex side of lobes throughout development. Interestingly, some areas of wall that did not initially have microtubule foci at day 1 formed new microtubule bands at later time periods on parts of the wall that were still straight and became lobes after this time. Our data confirm the hypothesis of Panteris and Galatis (2005) that the combination of alternating microtubule-rich regions on the convex side of lobes and microtubule-free regions on the concave side adjacent to periclinal walls predicts where lobes will form and are persistent during lobe growth.

However, it is unclear if other cellular components concentrate to promote the expansion of the periclinal wall on the concave side of lobes. Since previous studies using GFP-mTalin indicate that actin patches at the anticlinal wall on the concave side of lobes are instrumental to lobe development (Fu et al., 2002; Li et al., 2003; Mathur et al., 2003b; Djakovic et al., 2006; Xu et al., 2010), we expected that cortical actin filaments could also be concentrated adjacent to the periclinal wall. However, we did not observe broad

Figure 7. (continued).

middle row is a digital outline of the cell in which the cell area is colored, and the bottom row shows thin-plate spline analysis of differential growth in the periclinal cell walls between consecutive days. Bars = 50 μm.

(B) Changes in the mean area, perimeter, circularity, number of lobes, and the fold change in the number of lobes per perimeter from control and inhibitor treated cells from day 1 to 3. Error bars are SE of the mean and $n = 4$ cotyledons per treatment (with five cells from each cotyledon). Different letters represent statistically significant differences ($P < 0.05$, repeated measures ANOVA).

patches of filamentous actin at the anticlinal wall on the concave side of developing lobes. At days 2 and 3, actin filament bundles were significantly enriched on the convex side of lobes adjacent to the periclinal wall and were possibly parallel to microtubule bands at these sites. This difference in actin localization may be a result of the different GFP-tagged actin binding proteins used to highlight actin filaments within pavement cells. Actin filaments tagged with GFP-fABD2, used in this study, tend to be less bundled and exhibit faster dynamics than those tagged with GFP-mTalin, another actin-bundling protein (Sheahan et al., 2004; Holweg, 2007; Dyachok et al., 2014). Here, GFP-fABD2-tagged filamentous actin arrays changed in their distribution over 7 h, but in a previous study using wild-type pavement cells transiently expressing GFP-mTalin, the distribution of actin filaments showed little change over a 10-h period (Fu et al., 2002). It is possible that the broad actin patches observed in pavement cells expressing GFP-mTalin could be an artifact of the higher bundling capacity of mTalin, compared with GFP-fABD2. Cortical actin filaments are highly dynamic (Staiger et al., 2009), so unless they are stabilized by interactions with an actin binding protein, it is unlikely that they would remain concentrated in the cortical cytoplasm at the concave side of developing lobes. Other proteins known to be involved in lobe formation at the anticlinal wall could also be active at the periclinal wall. Likely candidates include those in a signaling cascade involving ROP2, RIC4, or SCAR1, although fluorescent visualization of these proteins suggests they do not extend far onto the outer periclinal wall at the concave side of lobes (Fu et al., 2005; Dyachok et al., 2008).

Although we did not observe concentrations of actin filaments at the concave side of lobes during their development, disruption of actin filaments at the earliest stages of pavement cell development hampered cell growth and fewer lobes were initiated. Thus, unlike the actin filaments involved in the tip growth of pollen tubes (Fu et al., 2001), concentrations of actin filaments seen by other authors at developing lobes in pavement cells may not be determining or reinforcing the site of lobe initiation (Fu et al., 2002, 2005; Lin et al., 2015). Instead, a cell may require functional actin filaments to indirectly initiate lobes and to assist in the further growth of lobes, possibly through transport of vesicles containing cell wall precursors or signaling proteins, such as ROP (Fu et al., 2005) or auxin binding protein 1 (Xu et al., 2010), to sites on the plasma membrane where new lobes will form. This agrees with the model of Panteris and Galatis (2005) that the role of actin filaments in lobe formation may be in the further expansion of a lobe. Additionally, we could predict sites of future lobe formation from concentrations of microtubules adjacent to the periclinal wall and the disruption of microtubules with oryzalin almost completely inhibited the initiation of new lobes and the growth of existing lobes. Cells with permanently altered microtubule arrays, such as in the MAP mutants *clasp-1* or *ric1-1*, display broader or fewer lobes and the central region of the cell between the convex side of lobes is wider (Fu et al., 2005; Ambrose et al., 2007; Ambrose and Wasteneys, 2008). Application of oryzalin to developing pavement cells resulted in the formation of fewer lobes and the middle of the cell expanded more than the controls. Overall, our data suggest that both actin filaments and microtubules are necessary for the initiation of lobes and formation of pavement cell shape.

METHODS

Growing Conditions

Wild-type *Arabidopsis thaliana* (Col-0) seeds and those expressing GFP fusion proteins were sterilized in 1% bleach for 10 min and imbibed at 4°C for 2 d. They were grown on 1× Murashige and Skoog salts, 1% sucrose, and 0.8% bacteriological agar (Oxoid brand; Thermo Fisher Scientific Australia) at 22°C on a 16-h-day:8-h-night cycle.

Imaging Pavement Cell Growth over Time

To visualize cell outlines, a 1 μM solution of 3 kD fluorescein conjugated dextran (Molecular Probes) was applied to the adaxial cotyledon surface and pavement cells were imaged using blue fluorescent light (filter set number 487910) on an Axiophot epifluorescence microscope with a 20× LD Achroplan objective lens with a numerical aperture of 0.4 (Carl Zeiss). For each cotyledon, a series of 30 to 60 images through multiple focal planes was processed into a 2D projection using the Stack Focuser plug-in in Fiji (built using ImageJ 1.44i; http://fiji.sc/wiki/index.php/Fiji). Each cotyledon was exposed to fluorescent light for less than 5 min. Cotyledons were rinsed with sterile milliQ water, and the seedlings returned to normal growth conditions. This was repeated after 24 and 48 h.

Cell Shape Metrics

At day 1, five nonadjacent cells with paradermal cross-sectional areas of 350 to 2000 μm^2 were selected from the base of each cotyledon. Outlines of the cells on days 1, 2, and 3 were traced from the 2D projections using the GNU Image Manipulation Program (GIMP) 2.6.11 (www.gimp.org/). In addition, the outlines of a group of 81 contiguous cells at the base of one cotyledon were traced for each day.

To map how individual cells grew, cell outlines were analyzed using the AnalyzeSkeleton plug-in in Fiji (Arganda-Carreras et al., 2010). The positions of wall junctions between neighboring cells, length of the anticlinal wall segments between two wall junctions, and the Euclidean distance between wall junctions were identified. Area, perimeter, number of lobes, and circularity [4π(area/perimeter^2)] were determined automatically for each cell using custom batch processing software (github.com/armour-william/Skeleton-analysis-of-cells). Automatic counts of the number of lobes used skeleton analysis (Le et al., 2006; Zhang et al., 2008, 2011; Staff et al., 2012). Lobes were also counted manually for each cell and included both convex and concave lobes.

Application of Fluorescent Landmarks

Homologous landmarks were applied to the adaxial surface of Arabidopsis cotyledons by spraying them with a 1:2 solution of fluorescent orange paint (Humbrol enamel paint #209:Humbrol enamel thinner AC7500; Hornby Hobbies). Seedlings were sprayed at a distance of 110 mm from an airbrush nozzle at a pressure of 140 kPa using a Sparmax airbrush (set at 5 turns of the tail screw) and air compressor (SP-35C and AC100, respectively; Dwing Hwa Co.). The seedlings were passed under the airbrush at a speed of 7 cm s^{-1}. Control seedlings were sprayed with air alone.

Thin-Plate Spline Analysis

Thin-plate spline analysis was used to investigate changes in pavement cell shape and size over time using PAST 2.10 (http://folk.uio.no/ohammer/past/). Input homologous landmarks included fluorescent dots affixed to the cell surface, cell wall junctions, or lobe tips. An alternative approach not requiring application of homologous landmarks used the input of the cell wall junctions and computed loci at 0.5-μm intervals along each of a cell's anticlinal wall segments at day 1. The locations of these computed loci at

days 2 and 3 were calculated assuming uniform expansion along each anticlinal wall segment using the following formula:

$$d = w/0.5\ \mu m$$

where d is desired number of loci in an anticlinal wall segment rounded to the nearest integer and w is the length of each wall segment. The position of these d loci was calculated using the following slope-intercept formulae:

$$f(a) = m * a + [p - [m * d]]$$

$$m = (p - 1)/(d - 1)$$

where f(a) is the selected loci from the list of xy coordinate pairs that describe the cell outline on each day, p is the number of xy coordinate pairs in a section of wall, and m is the gradient of the slope. Thin-plate splines were then created in PAST 2.10 using these select input coordinates.

All analyses used a Procrustes transformation that preserved scale and removed the effect of translation and rotation. This transformation aligned the coordinates across all days to the same axes. The relative growth rate of the outer periclinal wall was calculated from the fold expansion rates produced by PAST 2.10 and is presented as a color scale within select thin-plate splines.

Visualizing Relative Cell Growth

Fluorescent dots, wall junctions, and lobe tips were used as homologous landmarks to calculate relative wall growth rates. In cases where externally applied fluorescent landmarks were originally near lobe tips, they showed limited lateral displacement along the anticlinal wall (Supplemental Figure 6), indicating that lobe tips could be used as homologous markers. Relative wall growth rates of the anticlinal and periclinal walls were visualized as a color scale using the following formulae:

$$R_x = \ln(x_{t+dt}/x_t)/dt$$

$$c = 253R_x/(\max(R_x) + 1)$$

where R_x is the relative expansion rate, x is input trait such as the area or wall length at interval t, c is the color on a scale between 1 and 254, and max(R_x) is the largest value of R_x seen on all days. The pixel values 0 and 255 were reserved for the background and wall outline, respectively.

Imaging and Quantifying the Fluorescence of Actin Filaments and Microtubules in Pavement Cells

Seedlings expressing GFP-TUB6 or GFP-fABD2 were imaged using a Pascal confocal laser scanning system attached to an Axiovert inverted microscope (Carl Zeiss) using a 63× water immersion lens with a numerical aperture of 0.95, and images were captured with LSM5 software (Carl Zeiss). Individual pavement cells were imaged several times over 3 d. The cells were imaged in less than 5 min each time to minimize GFP bleaching and avoid negative effects of exposure to the fluorescent light. After imaging, seedlings were returned to the growth room.

The z-stack images of cells were rotated to the axis parallel to the epidermis with the interactive stack rotation plug-in in Fiji (built using ImageJ 1.44i; http://fiji.sc/wiki/index.php/Fiji). Cytoskeleton images were made of optical sections of the anticlinal wall at the middle of the cell and projections of serial sections of several focal planes of the cortical cytoplasm next to the outer periclinal wall. The fluorescence intensity of GFP-tagged microtubules or actin filaments adjacent to the periclinal or anticlinal walls at lobe tips was measured in five cells each using Photoshop CS5 Extended software (Adobe Systems). Fluorescence images were converted to grayscale and inverted, and then the fluorescence intensity was measured as the average gray-scale value in a region of interest. Within each cell, a total of seven lobes spanning three walls were analyzed. Boxed regions of equal sizes, representative of the size of each individual lobe, were placed perpendicularly to the concave and convex side of lobes on the periclinal wall. The fluorescence intensity of microtubules or actin filaments at lobe tips was measured and compared with regions of the anticlinal wall between lobe tips.

Application of Cytoskeletal Drugs

GFP-fABD2-tagged actin filaments were disrupted with 50 μM cytochalasin D (Szymanski et al., 1999) dissolved in 0.25% DMSO, and microtubules tagged with GFP-TUB6 were disrupted with 100 μM oryzalin (Szymanski et al., 1999) dissolved in 1% DMSO. The cytoskeletal filaments within targeted pavement cells were first imaged with the confocal microscope then treatment solution was applied to the surface of the cotyledon for two hours. Cytochalasin D was applied by placing directly on cotyledons (~0.2 μL). After 2 h, the cotyledons of GFP-fABD2 seedlings were rinsed for 5 min and then the cells reimaged immediately. This rinsing and imaging step was repeated at 24, 48, and 72 h after the initial imaging. Oryzalin was applied by inverting the seedlings so the cotyledon was in contact with the solution and was reapplied to treated cotyledons for a further 2 h at 2 h after the initial imaging. Oryzalin-treated seedlings were rinsed for 10 min and imaged at 0, 5, 24, 48, 96, and 120 h. A 1% DMSO control (applied and rinsed as in the oryzalin treatment), a 0.25% DMSO control (applied and rinsed as in the cytochalasin D treatment), and a control where milliQ water only was applied to cotyledon surfaces were also included.

Wild-type seedlings were treated with solutions as described above. All their cell walls were made visible via application of the fluorescent dextran and the cells were imaged at days 1, 2, and 3 on the Axiophot fluorescence microscope. Five cells from each of four cotyledons per treatment were selected for analysis and their area, perimeter, circularity, and number of lobes were determined at each time point.

Statistical Analyses

The area, perimeter, circularity, number of lobes, and change in the number of lobes per perimeter of cells, as a function of treatment and day, were analyzed using repeated measures ANOVA with treatment as the "between" factor. To solve heterogeneity of variance, values for area, perimeter, and change in the number of lobes per perimeter were log transformed, and values for circularity and number of lobes were square root transformed prior to data analysis. Differences between groups were determined using the Student-Newman-Kewls post-hoc test. The average fluorescence intensity of actin filaments and microtubules on the convex and concave side of lobes was compared using two-sample *t* tests. The intensity of actin filaments and microtubules along the anticlinal wall at and between lobes was compared using two-sample *t* tests.

Accession Numbers

Sequence data from this article can be found in the GenBank/EMBL data libraries under accession numbers AT4G26700 (*FIM1*) and AT5G12250 (*TUB6*).

Supplemental Data

Supplemental Figure 1. Spread of computed homologous landmarks along anticlinal wall segments over time from the lower half of the cell in Figure 1C.

Supplemental Figure 2. Comparison of two thin-plate spline analysis approaches.

Supplemental Figure 3. Actin filaments do not predict the site of lobe formation.

Supplemental Figure 4. Disruption to microtubule arrays using a chemical inhibitor, and their recovery.

Supplemental Figure 5. Disruption to actin filament arrays using a chemical inhibitor, and their recovery.

Supplemental Figure 6. Lateral displacement of externally applied landmarks near lobe tips.

ACKNOWLEDGMENTS

We thank Fiona Clissold (University of Sydney, Australia) for statistical advice for repeated measures ANOVA and three anonymous reviewers for their helpful comments and suggestions for additional experiments. This work was supported by an Australian Postgraduate Award to W.J.A.

AUTHOR CONTRIBUTIONS

W.J.A., D.A.B., and R.L.O. designed the research. W.J.A., D.A.B., and A.M.K.L. performed the research. W.J.A., D.A.B., and R.L.O. wrote the article.

Received April 15, 2014; revised July 16, 2015; accepted July 31, 2015; published August 21, 2015.

REFERENCES

Ambrose, C., Allard, J.F., Cytrynbaum, E.N., and Wasteneys, G.O. (2011). A CLASP-modulated cell edge barrier mechanism drives cell-wide cortical microtubule organization in Arabidopsis. Nat. Commun. **2:** 430.

Ambrose, J.C., Shoji, T., Kotzer, A.M., Pighin, J.A., and Wasteneys, G.O. (2007). The Arabidopsis CLASP gene encodes a microtubule-associated protein involved in cell expansion and division. Plant Cell **19:** 2763–2775.

Ambrose, J.C., and Wasteneys, G.O. (2008). CLASP modulates microtubule-cortex interaction during self-organization of acentrosomal microtubules. Mol. Biol. Cell **19:** 4730–4737.

Arganda-Carreras, I., Fernández-González, R., Muñoz-Barrutia, A., and Ortiz-De-Solorzano, C. (2010). 3D reconstruction of histological sections: Application to mammary gland tissue. Microsc. Res. Tech. **73:** 1019–1029.

Asl, L.K., Dhondt, S., Boudolf, V., Beemster, G.T.S., Beeckman, T., Inzé, D., Govaerts, W., and De Veylder, L. (2011). Model-based analysis of Arabidopsis leaf epidermal cells reveals distinct division and expansion patterns for pavement and guard cells. Plant Physiol. **156:** 2172–2183.

Baskin, T.I. (2001). On the alignment of cellulose microfibrils by cortical microtubules: a review and a model. Protoplasma **215:** 150–171.

Baskin, T.I., Meekes, H.T.H.M., Liang, B.M., and Sharp, R.E. (1999). Regulation of growth anisotropy in well-watered and water-stressed maize roots. II. Role of cortical microtubules and cellulose microfibrils. Plant Physiol. **119:** 681–692.

Basu, D., El-Assal, Sel.-D., Le, J., Mallery, E.L., and Szymanski, D.B. (2004). Interchangeable functions of Arabidopsis PIROGI and the human WAVE complex subunit SRA1 during leaf epidermal development. Development **131:** 4345–4355.

Basu, D., Le, J., El-Essal, Sel.-D., Huang, S., Zhang, C., Mallery, E.L., Koliantz, G., Staiger, C.J., and Szymanski, D.B. (2005). DISTORTED3/SCAR2 is a putative Arabidopsis WAVE complex subunit that activates the Arp2/3 complex and is required for epidermal morphogenesis. Plant Cell **17:** 502–524.

Basu, D., Le, J., Zakharova, T., Mallery, E.L., and Szymanski, D.B. (2008). A SPIKE1 signaling complex controls actin-dependent cell morphogenesis through the heteromeric WAVE and ARP2/3 complexes. Proc. Natl. Acad. Sci. USA **105:** 4044–4049.

Börstler, J., Lühken, R., Rudolf, M., Steinke, S., Melaun, C., Becker, S., Garms, R., and Krüger, A. (2014). The use of morphometric wing characters to discriminate female *Culex pipiens* and *Culex torrentium*. J. Vector Ecol. **39:** 204–212.

Brembu, T., Winge, P., Seem, M., and Bones, A.M. (2004). NAPP and PIRP encode subunits of a putative wave regulatory protein complex involved in plant cell morphogenesis. Plant Cell **16:** 2335–2349.

Burian, A., Ludynia, M., Uyttewaal, M., Traas, J., Boudaoud, A., Hamant, O., and Kwiatkowska, D. (2013). A correlative microscopy approach relates microtubule behaviour, local organ geometry, and cell growth at the Arabidopsis shoot apical meristem. J. Exp. Bot. **64:** 5753–5767.

Djakovic, S., Dyachok, J., Burke, M., Frank, M.J., and Smith, L.G. (2006). BRICK1/HSPC300 functions with SCAR and the ARP2/3 complex to regulate epidermal cell shape in Arabidopsis. Development **133:** 1091–1100.

Dyachok, J., Shao, M.R., Vaughn, K., Bowling, A., Facette, M., Djakovic, S., Clark, L., and Smith, L. (2008). Plasma membrane-associated SCAR complex subunits promote cortical F-actin accumulation and normal growth characteristics in Arabidopsis roots. Mol. Plant **1:** 990–1006.

Dyachok, J., Sparks, J.A., Liao, F., Wang, Y.-S., and Blancaflor, E.B. (2014). Fluorescent protein-based reporters of the actin cytoskeleton in living plant cells: fluorophore variant, actin binding domain and promoter considerations. Cytoskeleton (Hoboken) **71:** 311–327.

Elsner, J., Michalski, M., and Kwiatkowska, D. (2012). Spatiotemporal variation of leaf epidermal cell growth: a quantitative analysis of *Arabidopsis thaliana* wild-type and triple cyclinD3 mutant plants. Ann. Bot. (Lond.) **109:** 897–910.

Fu, Y., Gu, Y., Zheng, Z., Wasteneys, G., and Yang, Z. (2005). Arabidopsis interdigitating cell growth requires two antagonistic pathways with opposing action on cell morphogenesis. Cell **120:** 687–700.

Fu, Y., Li, H., and Yang, Z. (2002). The ROP2 GTPase controls the formation of cortical fine F-actin and the early phase of directional cell expansion during Arabidopsis organogenesis. Plant Cell **14:** 777–794.

Fu, Y., Wu, G., and Yang, Z. (2001). Rop GTPase-dependent dynamics of tip-localized F-actin controls tip growth in pollen tubes. J. Cell Biol. **152:** 1019–1032.

Geitmann, A., and Ortega, J.K.E. (2009). Mechanics and modeling of plant cell growth. Trends Plant Sci. **14:** 467–478.

Gunz, P., Mitteroecker, P., Neubauer, S., Weber, G.W., and Bookstein, F.L. (2009). Principles for the virtual reconstruction of hominin crania. J. Hum. Evol. **57:** 48–62.

Hamant, O., Heisler, M.G., Jönsson, H., Krupinski, P., Uyttewaal, M., Bokov, P., Corson, F., Sahlin, P., Boudaoud, A., Meyerowitz, E.M., Couder, Y., and Traas, J. (2008). Developmental patterning by mechanical signals in Arabidopsis. Science **322:** 1650–1655.

Holweg, C.L. (2007). Living markers for actin block myosin-dependent motility of plant organelles and auxin. Cell Motil. Cytoskeleton **64:** 69–81.

Hush, J.M., and Overall, R.L. (1991). Electrical and mechanical fields orient cortical microtubules in higher plant tissues. Cell Biol. Int. Rep. **15:** 551–560.

Hush, J.M., Hawes, C.R., and Overall, R.L. (1990). Interphase microtubule reorientation predicts a new cell polarity in wounded pea roots. J. Cell Sci. **96:** 47–61.

Jarvis, M.C., Briggs, S.P.H., and Knox, J.P. (2003). Intercellular adhesion and cell separation in plants. Plant Cell Environ. **26:** 977–989.

Kalve, S., Fotschki, J., Beeckman, T., Vissenberg, K., and Beemster, G.T.S. (2014). Three-dimensional patterns of cell division and expansion throughout the development of *Arabidopsis thaliana* leaves. J. Exp. Bot. **65:** 6385–6397.

Korn, R.W. (1976). Concerning the sinuous shape of leaf epidermal cells. New Phytol. **77:** 153–161.

Le, J., El-Assal, Sel.-D., Basu, D., Saad, M.E., and Szymanski, D.B. (2003). Requirements for Arabidopsis ATARP2 and ATARP3 during epidermal development. Curr. Biol. **13:** 1341–1347.

Le, J., Mallery, E.L., Zhang, C., Brankle, S., and Szymanski, D.B. (2006). Arabidopsis BRICK1/HSPC300 is an essential WAVE-complex subunit that selectively stabilizes the Arp2/3 activator SCAR2. Curr. Biol. **16:** 895–901.

Li, S., Blanchoin, L., Yang, Z., and Lord, E.M. (2003). The putative Arabidopsis arp2/3 complex controls leaf cell morphogenesis. Plant Physiol. **132:** 2034–2044.

Lin, D., Ren, H., and Fu, Y. (2015). ROP GTPase-mediated auxin signaling regulates pavement cell interdigitation in *Arabidopsis thaliana.* J. Integr. Plant Biol. **57:** 31–39.

Mathur, J. (2004). Cell shape development in plants. Trends Plant Sci. **9:** 583–590.

Mathur, J. (2006). Local interactions shape plant cells. Curr. Opin. Cell Biol. **18:** 40–46.

Mathur, J., Mathur, N., Kernebeck, B., and Hülskamp, M. (2003a). Mutations in actin-related proteins 2 and 3 affect cell shape development in Arabidopsis. Plant Cell **15:** 1632–1645.

Mathur, J., Mathur, N., Kirik, V., Kernebeck, B., Srinivas, B.P., and Hülskamp, M. (2003b). Arabidopsis CROOKED encodes for the smallest subunit of the ARP2/3 complex and controls cell shape by region specific fine F-actin formation. Development **130:** 3137–3146.

Nakamura, M., Naoi, K., Shoji, T., and Hashimoto, T. (2004). Low concentrations of propyzamide and oryzalin alter microtubule dynamics in Arabidopsis epidermal cells. Plant Cell Physiol. **45:** 1330–1334.

Panteris, E., and Galatis, B. (2005). The morphogenesis of lobed plant cells in the mesophyll and epidermis: organization and distinct roles of cortical microtubules and actin filaments. New Phytol. **167:** 721–732.

Panteris, E., Apostolakos, P., and Galatis, B. (1993a). Microtubules and morphogenesis in ordinary epidermal cells of *Vigna sinensis* leaves. Protoplasma **174:** 91–100.

Panteris, E., Apostolakos, P., and Galatis, B. (1993b). Microtubule organization and cell morphogenesis in 2 semi-lobed cell-types of *Adiantum capillus-veneris* L. leaflets. New Phytol. **125:** 509–520.

Panteris, E., Apostolakos, P., and Galatis, B. (1994). Sinuous ordinary epidermal cells: behind several patterns of waviness, a common morphogenetic mechanism. New Phytol. **127:** 771–780.

Paredez, A.R., Somerville, C.R., and Ehrhardt, D.W. (2006). Visualization of cellulose synthase demonstrates functional association with microtubules. Science **312:** 1491–1495.

Polder, G., van der Heijden, G.W.A.M., Jalink, H., and Snel, J.F.H. (2007). Correcting and matching time sequence images of plant leaves using Penalized Likelihood Warping and Robust Point Matching. Comput. Electron. Agr. **55:** 1–15.

Qiu, J.-L., Jilk, R., Marks, M.D., and Szymanski, D.B. (2002). The Arabidopsis SPIKE1 gene is required for normal cell shape control and tissue development. Plant Cell **14:** 101–118.

Rosas, A., and Bastir, M. (2002). Thin-plate spline analysis of allometry and sexual dimorphism in the human craniofacial complex. Am. J. Phys. Anthropol. **117:** 236–245.

Saedler, R., Zimmermann, I., Mutondo, M., and Hülskamp, M. (2004). The Arabidopsis KLUNKER gene controls cell shape changes and encodes the AtSRA1 homolog. Plant Mol. Biol. **56:** 775–782.

Sampathkumar, A., Krupinski, P., Wightman, R., Milani, P., Berquand, A., Boudaoud, A., Hamant, O., Jönsson, H., and Meyerowitz, E.M. (2014). Subcellular and supracellular mechanical stress prescribes cytoskeleton behavior in Arabidopsis cotyledon pavement cells. eLife **3:** e01967.

Sheahan, M.B., Staiger, C.J., Rose, R.J., and McCurdy, D.W. (2004). A green fluorescent protein fusion to actin-binding domain 2 of Arabidopsis fimbrin highlights new features of a dynamic actin cytoskeleton in live plant cells. Plant Physiol. **136:** 3968–3978.

Staff, L., Hurd, P., Reale, L., Seoighe, C., Rockwood, A., and Gehring, C. (2012). The hidden geometries of the *Arabidopsis thaliana* epidermis. PLoS One **7:** e43546.

Staiger, C.J., Sheahan, M.B., Khurana, P., Wang, X., McCurdy, D.W., and Blanchoin, L. (2009). Actin filament dynamics are dominated by rapid growth and severing activity in the Arabidopsis cortical array. J. Cell Biol. **184:** 269–280.

Szymanski, D.B. (2014). The kinematics and mechanics of leaf expansion: new pieces to the Arabidopsis puzzle. Curr. Opin. Plant Biol. **22:** 141–148.

Szymanski, D.B., Marks, M.D., and Wick, S.M. (1999). Organized F-actin is essential for normal trichome morphogenesis in Arabidopsis. Plant Cell **11:** 2331–2347.

Wasteneys, G.O., Willingale-Theune, J., and Menzel, D. (1997). Freeze shattering: a simple and effective method for permeabilizing higher plant cell walls. J. Microsc. **188:** 51–61.

Watson, R.W. (1942). The effect of cuticular hardening on the form of epidermal cells. New Phytol. **41:** 223–229.

Xu, T., Wen, M., Nagawa, S., Fu, Y., Chen, J.G., Wu, M.J., Perrot-Rechenmann, C., Friml, J., Jones, A.M., and Yang, Z. (2010). Cell surface- and rho GTPase-based auxin signaling controls cellular interdigitation in Arabidopsis. Cell **143:** 99–110.

Zhang, C., Halsey, L.E., and Szymanski, D.B. (2011). The development and geometry of shape change in *Arabidopsis thaliana* cotyledon pavement cells. BMC Plant Biol. **11:** 27.

Zhang, C., Mallery, E.L., Schlueter, J., Huang, S., Fan, Y., Brankle, S., Staiger, C.J., and Szymanski, D.B. (2008). Arabidopsis SCARs function interchangeably to meet actin-related protein 2/3 activation thresholds during morphogenesis. Plant Cell **20:** 995–1011.

Zhang, X., Dyachok, J., Krishnakumar, S., Smith, L.G., and Oppenheimer, D.G. (2005). IRREGULAR TRICHOME BRANCH1 in Arabidopsis encodes a plant homolog of the actin-related protein2/3 complex activator Scar/WAVE that regulates actin and microtubule organization. Plant Cell **17:** 2314–2326.